AIRCRAFT ENGINE RESPONSE DUE TO FAN UNBALANCE AND TO THE PRESENCE OF "CONSUMED" GAPS IN THE ENGINE DURING THE PHASE OF WINDMILLING

B. Bernay
AEROSPATIALE MATRA AIRBUS,
31060 Toulouse Cedex 03, France

Abstract

When fan blade off and gaps in a Turbomachine occur, non-linear loads take place. After a transient phase the main rotor reaches a "windmilling" motion, inside some frequencies range. Jump and hysteresis phenomena are observed in this range.

The paper presents two models for the dynamical simulation of the windmilling motion. First, a simplified model is used for which analytic solutions are obtained. The results are compared to the numerical integration of a finite element model of the aircraft. Based on this analysis, an harmonic method has been developed to compute the jump frequency; a sensitivity study of the different parameters related to the jump phenomenon is performed.

1 Introduction

The design of large commercial jet aircraft has required the use of high by-pass engines with large fans. The size of these fans has steadily increased to accommodate the thrust required of successively larger aircraft and simultaneously to improve operating efficiency. It is then necessary to investigate the loads due to fan blade off.

After the fan blade off event, a transient phase occurs. During this phase, the main rotor ("LP rotor" or "Fan shaft"…) speed decreases rapidly. Then a stabilized phase occurs in which the main rotor reaches a "windmilling" motion inside some frequencies range depending on the velocity and on the altitude of the aircraft. During this motion, several contacts may occur. These contacts come from the unbalance produced by the fan blade off. This unbalance produces the bending of the shaft. (Lalanne and Ferraris, 1998).

Moreover, during the transient phase, where strong vibrations occur, some bearings ("fused" bearings) which are intended to support the LP rotor are broken. It results a reduction of the strong vibrations of the rotor induced by the fan blade off but on the other hand, the loss of these bearings leads to a larger precessional motion of the rotor and for some values of the rotational frequency, several impacts may occur.

A physical model with two degrees of freedom, which represents the rotor system with a bearing clearance has been proposed by Ehrich and O'Connor (1967). They showed the occurrence of jump and hysteresis phenomena due to the dynamic coupling between the rotor and the stator. Black reported his experimental observation of these phenomena (1967) and developed a model (1968) in which polar receptances are used to establish equilibrium conditions.

In this paper, we use the simplified model of Ehrich and O'Connor in which a snubbing stiffness is added in order to take into account the deformations occurring near the contact zone. In a second step the results of the time simulations based on a finite element model of the system {engine+aircraft} are presented. A parallel is made with the simplified model to understand the mechanism with "multigaps" which leads to the jump phenomenon. Finally a frequency method based on this analysis is developed to determine the frequency at which the jump phenomenon occurs ; this method allows sensitivity studies on the jump frequency to be performed.
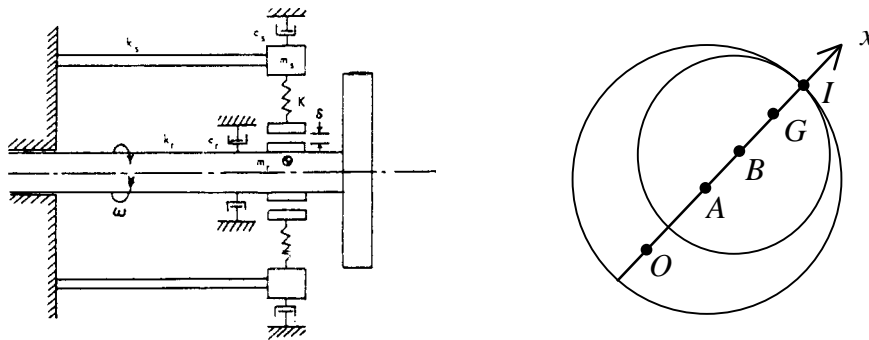
Fig 1 : Physical model of a rotor operating in bearing clearance with real stator dynamics

2 Simplified model

A simplified model for the dynamic behavior of a turbomachinery is shown in Fig. 1. (Ehrich and O'Connor, 1967).

A rotor of mass m_r is overhung by a symmetric shaft of stiffness k_r and fixed at one end. A stator of mass m_s is overhung by a symmetric shaft of stiffness k_s and also fixed at one end.

The rotor is modeled by a beam of center B, of radius r and of center of mass G offset from B by a distance ε : this unbalance is produced by the loss of fan blades. The stator is modeled by a disk of center A, of radius $r_1 = r + \delta$ (δ is the clearance), whose center of mass is assumed to be located at A (Fig. 1).

The friction forces are neglected and the motion is assumed to be synchronous and axisymmetric. Therefore only two degrees of freedom are sufficient to describe the motion of the rotor and the stator : the radial displacements r_r of the rotor and r_s of the stator. The three points A, B and G are on the same line $A\vec{x}$ ($A\vec{x}$ oriented in such a way that $\overline{BG} = \varepsilon\vec{x}$, with $\varepsilon > 0$).

When a contact occurs between the rotor and the stator (i.e. when $|r_s - r_r| > \delta$), the reaction force $\vec{R}$ exerted at the contact point I is directed along the line $A\vec{x}$ if no friction effects occur. In contrast with the study made in Ehrich and O'Connor, we assume that small penetration can occur near the contact point and a concentrated stiffness K is introduced. Thus, the model used in Ehrich and al. is obtained for K infinite.

We will first assume that energy dissipation on the rotor and stator structure is neglected :

$$c_r = c_s = 0 \qquad (1)$$

Two possible cases are then considered:

I. Case without contact :

In this case, we assume that $r_s = 0$ and $|r_r| < \delta$.

The reaction force $\vec{R}$ is absent. The resulting equations are as follows :

$$\begin{cases} r_s = 0 \\ -m_r\omega^2(r_r + \varepsilon) + k_r r_r = 0 \\ |r_r| < \delta \end{cases} \qquad (2),(3)(4)$$

Equation (3) gives :

$$\frac{r_r}{\varepsilon} = \frac{\omega^2}{\omega_r^2 - \omega^2} \qquad (5)$$

with:

$$\omega_r = (k_r / m_r)^{1/2} \qquad (6)$$

II. Case with contact :

In this case, $|r_r - r_s| \geq \delta$. Among the two possible cases, $r_r - r_s \geq \delta$ or $r_r - r_s \leq \delta$, only the first one is considered. Ehrich and al. (1967) has shown that the second possibility corresponding to a motion of the stator with a larger amplitude than the rotor is unstable. The $\vec{x}$ projection R of the reaction force $\vec{R}$ exerted at the contact point I on the rotor is given by :

$$R = -K(r_r - r_s - \delta) \qquad (7)$$

The resulting equations are then :

$$\begin{cases} K(r_r - r_s - \delta) = m_r\omega^2(r_r + \varepsilon) - k_r r_r \\ \qquad = -m_s\omega^2 r_s + k_s r_s \\ r_r - r_s \geq \delta \end{cases} \quad (8),(9)$$

From equation (8), we obtain the following expressions under condition (9) :

$$\frac{r_r}{\varepsilon} = \frac{\omega_s^2\left(-\mu\delta/\varepsilon - k_s/K\times\omega^2/\omega_s^2\right) + \omega^2\left(\mu\delta/\varepsilon - 1 + k_s/K\times\omega^2/\omega_s^2\right)}{k_s/K\times\left(\omega^2 - \omega_r^2\right) + \omega^2\left(1 + \mu - k_s/K\times\left(\omega^2 - \omega_r^2\right)/\omega_s^2\right) - 1 - \mu} \quad (10)$$

$$\frac{r_s}{\varepsilon} = \frac{\omega_r^2\,\delta/\varepsilon + \omega^2\left(-\delta/\varepsilon - 1\right)}{k_s/K\times\left(\omega^2 - \omega_r^2\right) + \omega^2\left(1 + \mu - k_s/K\times\left(\omega^2 - \omega_r^2\right)/\omega_s^2\right) - 1 - \mu} \quad (11)$$

with :

$$\mu = m_s/m_r \quad (12)$$

The behavior of the obtained solution depends on several parameters, namely $\mu, \dfrac{\delta}{\varepsilon}, \dfrac{K}{k_s}, \dfrac{\omega_r}{\omega_n}, \dfrac{\omega_s}{\omega_n}$ where :

$$\omega_n = \left(\frac{k_r + k_s}{m_r + m_s}\right)^{1/2} \quad (13)$$

As it is pointed in Ehrich and al. (1967), the case of a stator with a great stiffness is more interesting leading to the assumptions $\omega_r < \omega_n < \omega_s$. Moreover, when $\delta/\varepsilon \geq \left(1 - (\omega_r/\omega_n)^2\right)^{-1}$, particular interesting behaviors like jump and hysteresis phenomena occur. In (Fig. 2), the vibration responses of the system are shown assuming the following numerical data : $\omega_r/\omega_n = 0.5$, $\mu = 1.0$ (as follows $\omega_s/\omega_n \approx 1.35$), $\delta/\varepsilon = 2$ K/k_s taking different values between (1 and 1000). From these curves, we can make the following conclusions :

-when ω increases from 0.5 to 1, the total branch "2" (case with contact) is described, followed by a "jump down" (vertical asymptote) to join the branch "1" (case without contact).

-when the ω decreases from 1 to 0.5, branch "1" then "2" is followed, the latter being joined after a "jump up". This jump occurs when the clearance is reached (as $r_r = -\delta$) : it is thus the second intersection between the response curve of the rotor without contact and the curve of equation $r_r = -\delta$, that is :

$$\omega_{jump} = \omega_r \sqrt{\frac{\delta/\varepsilon}{\delta/\varepsilon - 1}} \quad (14)$$

- When K/k_s decreases, the amplitude of the jump up increases and branch "2" moves to the left and thus the jump down follows. The case $K/k_s = 1000$ (infinite) corresponds to the Ehrich's case.

We will now consider the case in which damping coefficients c_r and c_s are not neglected. The synchronization assumption is then no longer valid and an analytical solution for branch "2" is thus no longer available. On the other hand, we find the following expression for the first case without contact :

$$\frac{r_r}{\varepsilon} = \frac{\omega^2}{\sqrt{\left(\omega_r^2 - \omega^2\right)^2 + 4\omega^2\omega_r^2\xi_r^2}} \quad (15)$$

with :

$$\xi_r = \frac{c_r}{2m_r\omega_r} = \frac{c_r}{2\sqrt{k_r m_r}} \quad (16)$$

Following the same method as presented before (the "jump up" frequency corresponds to the second intersection between the response curve of the rotor without contact and the curve of equation $r_r = \delta$), the expression of ω_{jump} is found as :

$$\omega_{jump} = \omega_r \sqrt{\frac{1 - 2\xi_r^2 + \sqrt{4\xi_r^2(\xi_r^2 - 1) + \varepsilon^2/\delta^2}}{1 - \varepsilon^2/\delta^2}} \quad (17)$$

Branch "2" is obtained by solving dynamic equations of the system {rotor+stator+bearing}. This resolution will not be presented here. It can simply be noted here that the effect of the damping is, as usually observed, to smooth the responses and in particular to decrease the jump down frequency.

3   Mechanism leading to jump phenomena

In the following , a finite element model of the aircraft+engine is investigated in order to compare the results obtained from the simplified model. The engine is represented by a condensed finite element model (Guyan's condensation) of 500 dof. The condensed aircraft model (same condensation) is represented by 20000 dof. The modal analysis is made with 250 modes. In this analysis, the 250th mode has a frequency around 60 Hz, which allows correct analysis to be made up to 40 Hz. In fact the "windmilling" frequency range is [8 Hz ; 20 Hz].

In contrast with the simplified model in which only one contact may occur, four consumed clearances have to be considered here :

1. Two between the blades and the casing : between the fan and the fan casing and between the compressor blades (IPR), which are attached to the intermediate rotor IP, and the compressor casing (IPC).

2. A clearance between the rotor IP and the bearing casing (FBH).
3. A clearance between the LP and IP rotors.

Radial snubbing stiffness related to the reaction forces occurring when some of the four possible contacts are present are shown fig. 3. The fan-fan casing snubbing force is more complex than the other one, as the snubbing stiffness changes when the radial displacement grows (blade elastic buckling). Finally rubbing is not taken into account.

For a rotation frequency of the fan (or LP rotor) ω_0, the equation governing the aircraft+engine structure dynamics, expressed in the modal basis, is :

$$[\mu]\{\ddot{q}\}+\left([\beta]+[\Psi]^T[G(\omega_0)]\,[\Psi]\right)\{\dot{q}\}+[\gamma]\,\{q\}$$
$$=[\Psi]^T\left(\{F_{unbalance}(t)\}+\{F_{contact}(t)\}\right) \quad (\,18\,)$$

with :

- $[\mu]$, $[\beta]$ and $[\gamma]$, diagonal matrices 250×250, represent the modal mass, damping and stiffness.
- $[\Psi]$ is the mode shape matrix.
- $[G(\omega_0)]$ is the antisymmetric matrix of the gyroscopic effects. It contains n blocks if n points represent the LP rotor (the other rotors do not rotate during the windmilling phase), each one affected by a polar inertia Ip_i. The ith bloc is :

$$[G_i(\omega_0)]=\begin{bmatrix} 0 & \omega_0 Ip_i \\ -\omega_0 Ip_i & 0 \end{bmatrix} \quad (\,19\,)$$

- $\{F_{unbalance}(t)\}$ has only two components in the transverse (y) and vertical (z) directions with respect to the LP rotor axis :

$$F_{unbalance,y}(t)=m.r.\omega_0^{\,2}\cos(\omega_0.t) \quad (\,20\,)$$
$$F_{unbalance,z}(t)=m.r.\omega_0^{\,2}\sin(\omega_0.t) \quad (\,21\,)$$

m represents the blades off mass and r the eccentricity of the rotor cg from the rotor geometric centerline due to this blade loss.

The calculation of the term $\{F_{contact}(t)\}$ is obtained by a loop : from the computed relative radial displacements the contact forces are obtained (from the snubbing stiffness of the figure 3) and are then considered as excitation forces with the unbalance force. Then equation (18) is solved by a Runge-Kutta integration scheme to obtain the relative radial displacements.

Several simulations corresponding to a constant rotation frequency of the fan in the windmilling range [8 Hz ; 22 Hz] are performed. For each simulation the local peak amplitudes (Poincaré points) are shown, together with the Fourier transform of the displacements for waterfall chart (Ehrich, 1992). From the Poincare points method, a comparison with the response without contact is made.

To understand the mechanism which leads to the jump phenomenon, the transverse[1] relative displacements of the contact points due to the unbalance force only are calculated in the range [8 Hz ; 32 Hz], which is a larger frequency range than the windmilling frequency range to have an enlarged view of the phenomenon. Comparing these displacements and their clearance (for example $dy_{fan}-dy_{ca\sin g}$ and the first clearance) allows us to know if snubbing occurs.

As the unbalance force is harmonic these displacements are obtained by a frequency calculation. For example for the fan-fan casing relative displacement :

$$dy_{fan}(\omega)-dy_{ca\sin g}(\omega)$$
$$=\left([\Psi_{fan,y}]-[\Psi_{ca\sin g,y}]\right)[D(\omega_0)][\Psi]^T\{F_{unbalance}(\omega)\} \quad (\,22\,)$$

with :

- $[D(\omega_0)]=\left(-\omega_0^{\,2}.[\mu]\;+j\omega_0.\left([\beta]+[\Psi]^T[G(\omega_0)]\,[\Psi]\right)+[\gamma]\;\right)^{-1}$ $\quad (\,23\,)$
- $F_{unbalance,y}(\omega)=m.r.\omega_0^{\,2}\delta(\omega-\omega_0)$ $\quad (\,24\,)$
- $F_{unbalance,z}(\omega)=m.r.\omega_0^{\,2}\delta(\omega-\omega_0).(-j)$ $\quad (\,25\,)$
- $[\Psi_{fan,y}]$ and $[\Psi_{ca\sin g,y}]$ represent the lines of the matrix $[\Psi]$ which correspond to the degrees of freedom in the y direction at the fan and fan casing points that can be in contact.

In figure 4, the amplitude of these displacements is compared with the Poincaré points of the corresponding displacements in response to the unbalance force and to the snubbing forces when they take place, and with their respective clearances.

Two resonance peaks appear corresponding to :

- at 8.5 Hz : LP rotor first bending mode.
- at 25 Hz : IP rotor first bending mode.

An antiresonance also appears for the LP rotor – IP rotor relative displacement amplitude : the

---

[1] The simulations show that the amplitude of the vertical and transversal motions are quasi equal for each rotation frequency in the windmilling range ; that means that the dynamic stiffness of the system is symmetric.

displacement is less than the clearance in the range [17 Hz ; 21 Hz]. The IP rotor -FBH and IPR-IPC displacements are similar : "IP rotor" and "IPR" correspond to two near points on the same shaft and the casing (FBH and IPC) displacement amplitudes are small in comparison with IP rotor displacement amplitudes.

For a rotational frequency ω_0 between 17 and 18.2 Hz, the four relative displacement amplitudes are less than their respective clearance : the Poincaré points are then on the curve (C) corresponding to the displacement amplitude due to the unbalance force.

Under 17 Hz, the LP rotor-IP rotor displacement amplitude is less than its clearance δ_2 : the two rotating parts are in contact and the corresponding Poincaré points separate from the curve (C).

At 15 Hz the IPC-IPR displacement amplitude reaches its clearance δ_4 ; the jump phenomenon then takes place. As in the case of the simplified model already considered, the jump phenomenon takes place when the clearance between fixed (IPC) and rotating (IPR) parts is consumed. The difference between this industrial case and the model lies in the preliminary phase when the two rotors come into contact. The "jump" frequency is then obtained at the intersection of the following two curves :
- The IPC-IPR displacement amplitude, that is the response to the unbalance force <u>and</u> the snubbing force of the two rotors ("LP-IP").
- The curve of equation : $dy_4 = \delta_4$.

At 18.2 Hz the IPC-IPR displacement amplitude reaches its clearance : the two parts are in contact and the Poincaré points of this displacement separates from the curve (C). This diminishes the LP rotor-IP rotor displacement amplitude. The influence on the fan-fan casing displacement amplitude is smaller.

4 Harmonic method to determine the jump frequency

The results obtained from the integration of the finite element model show that the jump phenomenon occurs when the 4th clearance δ_4 (IPR-IPC contact) is reached while the 2nd clearance δ_2 (LP-IP contacts) was already reached. The time integration of the finite element model for several rotational frequencies of the fan needs high computer time. In order to perform a sensitivity study of the jump phenomenon when the values of the two clearances (LP-IP and IPR-IPC) are changed, the finite element model is solved in frequency domain, assuming that the response is harmonic, with the same frequency ω_0 as the rotational frequency of the fan. From formulas (24) (25), it is clear that the unbalance force is harmonic, with the frequency ω_0. Assuming that the mechanism leading to the jump is the same (first the LP-IP clearance is reached and then jump phenomenon occurs when the IPR-IPC clearance is reached) even if the values of these clearances are slightly changed, we have to take into account in the finite element model the LP-IP contact force. The experimental data give only the value of the radial stiffness K_2 corresponding to the LP-IP contact. It results that the contact force $\overrightarrow{F_2}$ is given by its transverse F_{2y} and vertical F_{2z} components in a plane perpendicular to the direction of the LP,IP rotor axis by the following expressions :

$F_{2y}(t) =$
$$K_2.(\sqrt{(dy_{LP}(t) - dy_{IP}(t))^2 + (dz_{LP}(t) - dz_{IP}(t))^2} - \delta_2).\cos\theta \quad (26)$$
$F_{2z}(t) =$
$$K_2.(\sqrt{(dy_{LP}(t) - dy_{IP}(t))^2 + (dz_{LP}(t) - dz_{IP}(t))^2} - \delta_2).\sin\theta \quad (27)$$
with :
$$\theta = Arc\tan\left(\frac{dz_{IP}(t) - dz_{LP}(t)}{dy_{IP}(t) - dy_{LP}(t)}\right) \quad (28)$$

dy_{LP}, dy_{IP} and dz_{LP}, dz_{IP} correspond to the displacements in the transverse and vertical direction of the LP and IP rotor points in contact.

However, the results obtained from the time simulation at constant rotation frequency show that when the two shafts are in contact, the radial relative displacement between the two contact points of the LP and IP rotor is nearly constant, leading to the following assumption :

$$\begin{cases} dy_{LP}(t) = dr_{LP}.\cos(\omega_0.t + \varphi(\omega_0)) \\ dz_{LP}(t) = dr_{LP}.\sin(\omega_0.t + \varphi(\omega_0)) \\ dy_{IP}(t) = dr_{IP}.\cos(\omega_0.t + \varphi(\omega_0)) \\ dz_{IP}(t) = dr_{IP}.\sin(\omega_0.t + \varphi(\omega_0)) \end{cases} \quad (29)$$

the precession angle θ is :

$$\theta = \omega_0.t + \varphi(\omega_0) \quad (30)$$

where $\varphi(\omega_0)$ is the angle between the position vector of the two points and the unbalance force.

The transverse and vertical components of the LP-IP snubbing force then become :

$$F_{2y}(t) = K_2.[dy_{LP}(t) - dy_{IP}(t) - \delta_2.\cos(\omega_0.t + \varphi(\omega_0))] \quad (31)$$

$$F_{2z}(t) = K_2.[dz_{LP}(t) - dz_{IP}(t) - \delta_2.\sin(\omega_0.t + \varphi(\omega_0))] \quad (32)$$

With these assumptions, these components are also expressed linearly as a function of the snubbing shaft points. The Fourier transform of these components is then easily determined :

$$F_{2y}(\omega) = K_2.(dy_{LP}(\omega) - dy_{IP}(\omega) - \delta_2.e^{j\varphi(\omega_0)}.\delta(\omega - \omega_0)) \quad (33)$$

$$F_{2z}(\omega) = K_2.(dz_{LP}(\omega) - dz_{IP}(\omega) - \delta_2.e^{j\varphi(\omega_0)}.(-j).\delta(\omega - \omega_0)) \quad (34)$$

The "frequency" expressions obtained for the unbalance effort and the LP-IP snubbing force are then put into the Fourier transform of the dynamic equation expressed in the modal basis :

$$\left(-\omega^2.[\mu_i] + j\omega.([\beta_i] + [\Psi]^T [G(\omega)] [\Psi]) + [\gamma_i]\right)\{q(\omega)\} =$$
$$[\Psi]^T (\{F_{unbalance}(\omega)\} + \{F_2(\omega)\}) \quad (35)$$

The detailed calculations are presented in the appendix.

This method is applied on the sensitivity analysis of the 2nd and 4th clearances on the jump frequency. In fact, in comparison with the initial time method, this one allows us to understand better the role of each gap. The variation of the IPR-IPC clearance simply corresponds to the translation of the curve of equation $dy_4 = \delta_4$. On the other hand, as we calculate the relative IPR-IPC displacement amplitude, that is the response to the unbalance force <u>and</u> snubbing force of the two rotors ("LP-IP"), the number of "frequency" simulations is equal to the number of chosen LP-IP clearance values.

These values are 75%, 80%,... 135% of the initial gap, so 13 simulations (figure 5) have to be made. The limit values are chosen in order to respect the mechanism described before : a frequency range where no contact occurs exist ; the 2nd clearance then the 4th one is reached during the deceleration. So for each LP-IP clearance value the corresponding values for the IPR-IPC clearance are determined (for instance for 80 % of δ_2, δ_4 can vary from 120 % to 135 %).

We observed that, as the LP-IP clearance value diminishes, the curve of the IPR-IPC displacement amplitude moves to the right side and the resonance peak increases: it is due to the augmentation of the equivalent snubbing stiffness. The results of this sensitivity study can be seen in the figure 6. This figure proves the

sensitivities of the two clearances : for 160% of the two gaps, the jump frequency decreases to 11 Hz.

5 Conclusion and prospects

A parallel has been found between the dynamic behavior of the simplified model and that of the FE integrated engine+aircraft model. It allows a "frequency" method of jump frequency determination to be developed and then a sensitivity study on two consumed gaps to be made.

Concerning the simplified model an analytical solution of the steady motion with damping will be developed, based on Yamamoto (1954).

The blades to casing contact model will be refined as Padovan and Choy (1987) and the rubbing will be taken into account. The utilization of a FE model of the blades is studied.

The modal basis is formed by "failed engine" modes, after the fused bearings have broken. A component mode synthesis will be studied with component boundary coordinates at the contact points (Berthillier and al., 1998).

An analysis of the hysteresis phenomenon will be made : we will show that a disturbance on the engine+aircraft system (for example a gust which could occur during the flight) can cause the "hang" of the second stability branch, as in the simplified model.

Finally, a better understanding of dynamic phenomena is expected with tests on a simplified motor rig.

References

[1] Black H. F. "Synchronous Whirling of a Shaft Within a Radially Flexible Annulus Having Small Radial Clearance". *IMechE* Paper 4, Vol. 191, pp. 65-73, 1966-67.

[2] Black H. F. "Interaction of a Whirling Rotor With a Vibration Stator Across a Clearance Annulus". *Journal Mechanical Engineering Science,* Vol. 10 No 1, pp. 1-12, 1968.

[3] Berthillier M., Dupont C., Mondal R. "Blades Forced Response Analysis with Friction Dampers". ASME *Journal of Vibration and Acoustics,* Vol. 120, No. 2, pp. 468-474, April 1998.

[4] Ehrich F. F. and O'Connor J. J. "Stator Whirl With Rotors in Bearing Clearance". ASME *Journal of Engineering for Industry,* pp. 381-390, 1967.

[5] Lalanne M. and Ferraris G. *"Rotordynamics Prediction in Engineering"*. John Whiley and Sons, 1998.

[6] Padovan J. and Choy F. K. "Nonlinear Dynamics of Rotor/Blade/Casing Rub Interactions". ASME *Journal of Turbomachinery,* Vol. 109, pp. 527-534, 1987.

[7] Yamamoto T. T. "On Critical Speeds of a Shaft" *Memoirs of the Faculty of Engineering, Nagoya (Japan) University,* Vol. 6, No 2., pp. 160-170, 1954.

Appendix

In equation (35), the term that has to be calculated is $[\Psi]^T\{F_{LP-IP}(\omega)\}$. With expressions (33) and (34), and as :

$$\begin{cases} dy_{LP}(\omega) = [\Psi_{LP,y}]\{q(\omega)\} \\ dz_{LP}(\omega) = [\Psi_{LP,z}]\{q(\omega)\} \\ dy_{IP}(\omega) = [\Psi_{IP,y}]\{q(\omega)\} \\ dz_{IP}(\omega) = [\Psi_{IP,z}]\{q(\omega)\} \end{cases} \quad (36)$$

this term becomes :

$$[\Psi]^T\{F_{LP-IP}(\omega)\} = -[\Delta\gamma]\{q(\omega)\}\delta(\omega-\omega_0) + [\Psi]^T\{F_{LP-IP}(\omega,\varphi)\}_2 \quad (37)$$

with :

$$[\Delta\gamma] = K_{LP-IP}\left(([\Psi_{LP,y}]-[\Psi_{IP,y}])^T.([\Psi_{LP,y}]-[\Psi_{IP,y}]) + ([\Psi_{LP,z}]-[\Psi_{IP,z}])^T.([\Psi_{LP,z}]-[\Psi_{IP,z}])\right) \quad (38)$$

and :

$$[\Psi]^T\{F_{LP-IP}(\omega,\varphi)\}_2 =$$
$$K_{LP-IP}.\delta_{LP-IP}.e^{j\varphi(\omega_0)}.\delta(\omega-\omega_0).([\Psi_{LP,y}]^T - j[\Psi_{LP,z}]^T - [\Psi_{IP,y}]^T + j[\Psi_{IP,z}]^T) \quad (39) \text{ and } (40)$$

The term $\varphi(\omega_0)$ is obtained by the intersection of two curves whose equations are :

$$\begin{cases} \varphi \to \varphi \\ \varphi \to \arg\left([H(\omega_0)]_{contact}.(\{F_{unbalance}(\omega_0)\} + \{F_{LP-IP}(\omega_0,\varphi)\}_2)\right) \end{cases} \quad (41)$$

with :

$$[H(\omega_0)]_{contact} = [\Psi](-\omega_0^2.[\mu] + j\omega_0.([\beta] + [\Psi]^T[G(\omega_0)][\Psi]) + [\gamma] + [\Delta\gamma])^{-1}[\Psi]^T \quad (42)$$

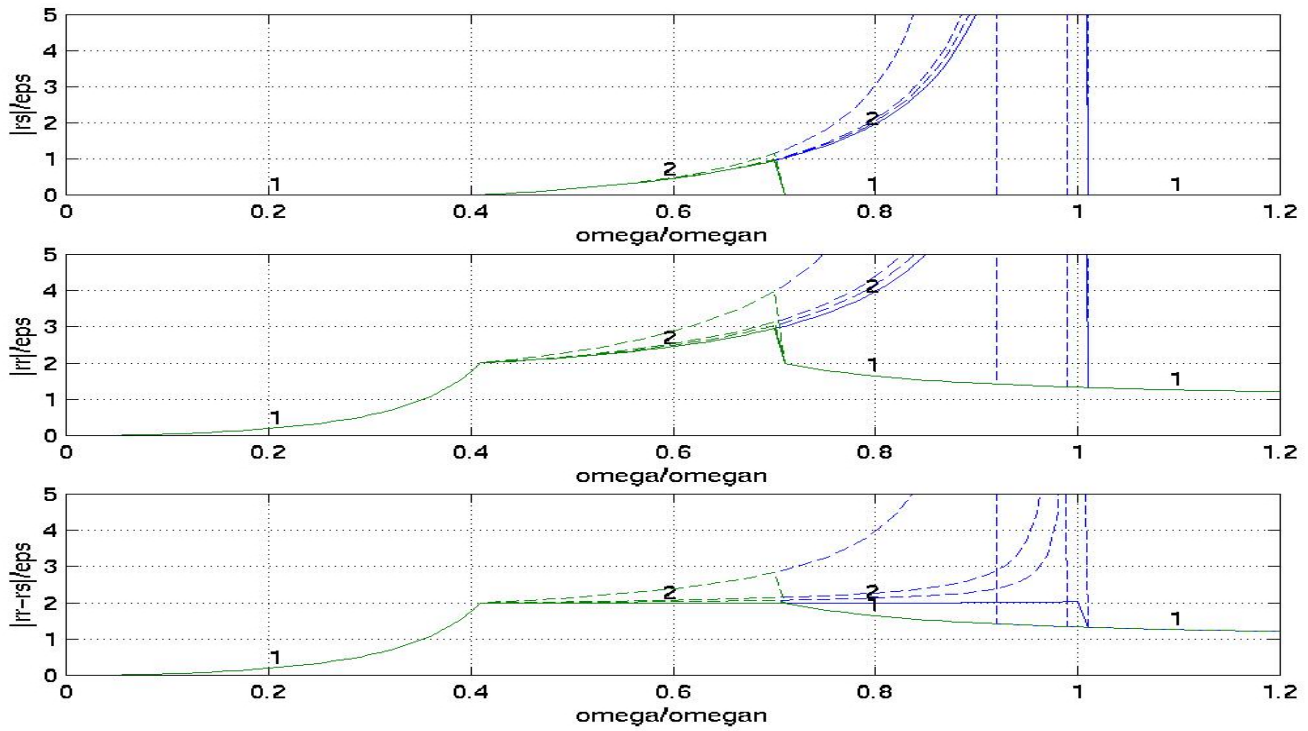**Fig 2 : Normalized stator, rotor and relative amplitudes for** $K/k_s \in [1000,10,5,1]$ ($K/k_s = 1000$ **in solid lines).**
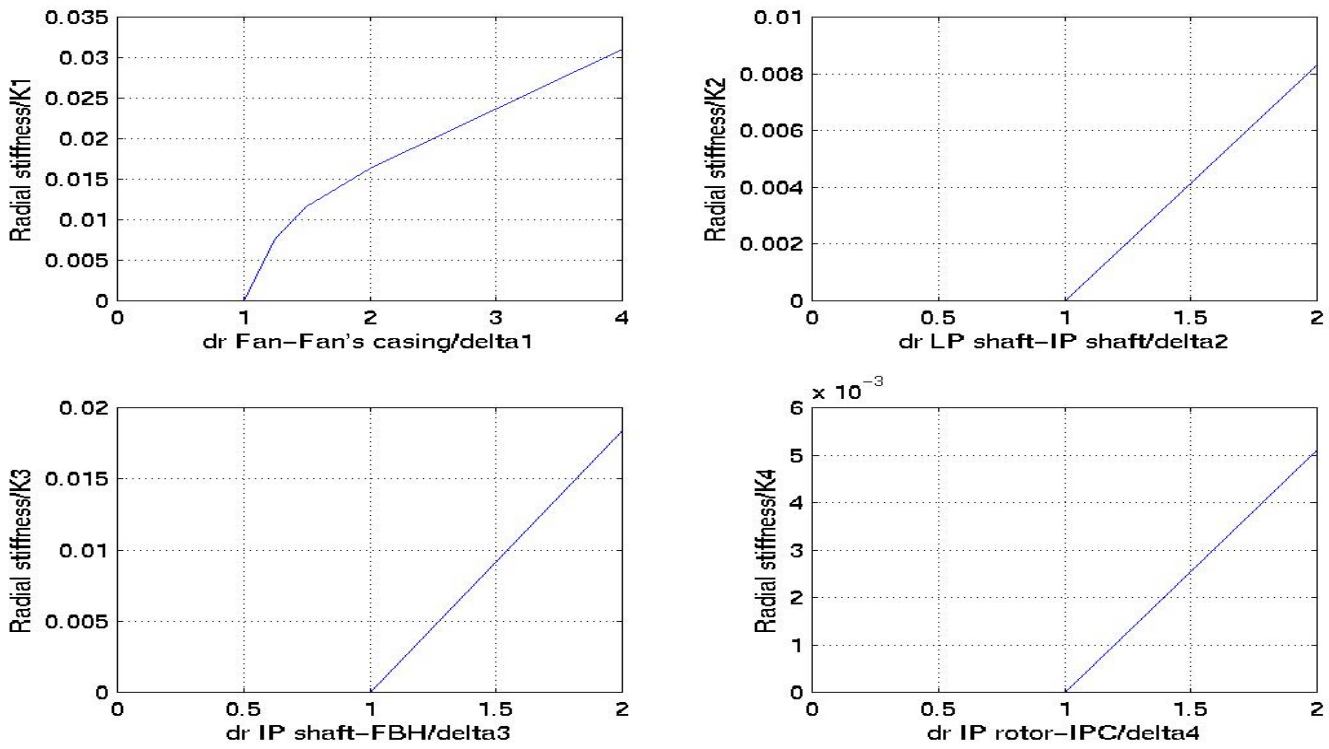**Branch "1" : case without contact. Branch "2" : case with contact.**
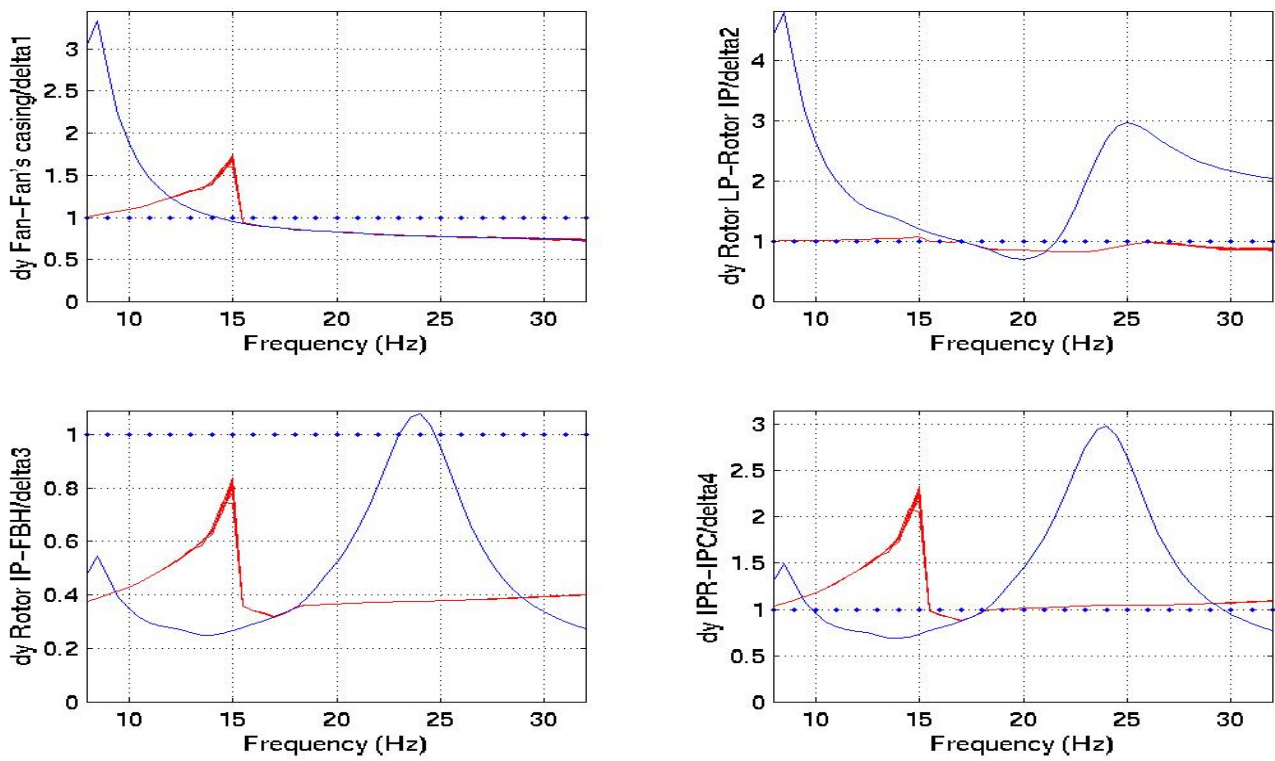

Fig 3 : Radial snubbing stiffness

Fig 4 : Transverse relative displacements of the contact points (plus their clearances) :
1. Due to the unbalance force (in blue) 2. Due to the unbalance and snubbing forces (Poincaré points in red)
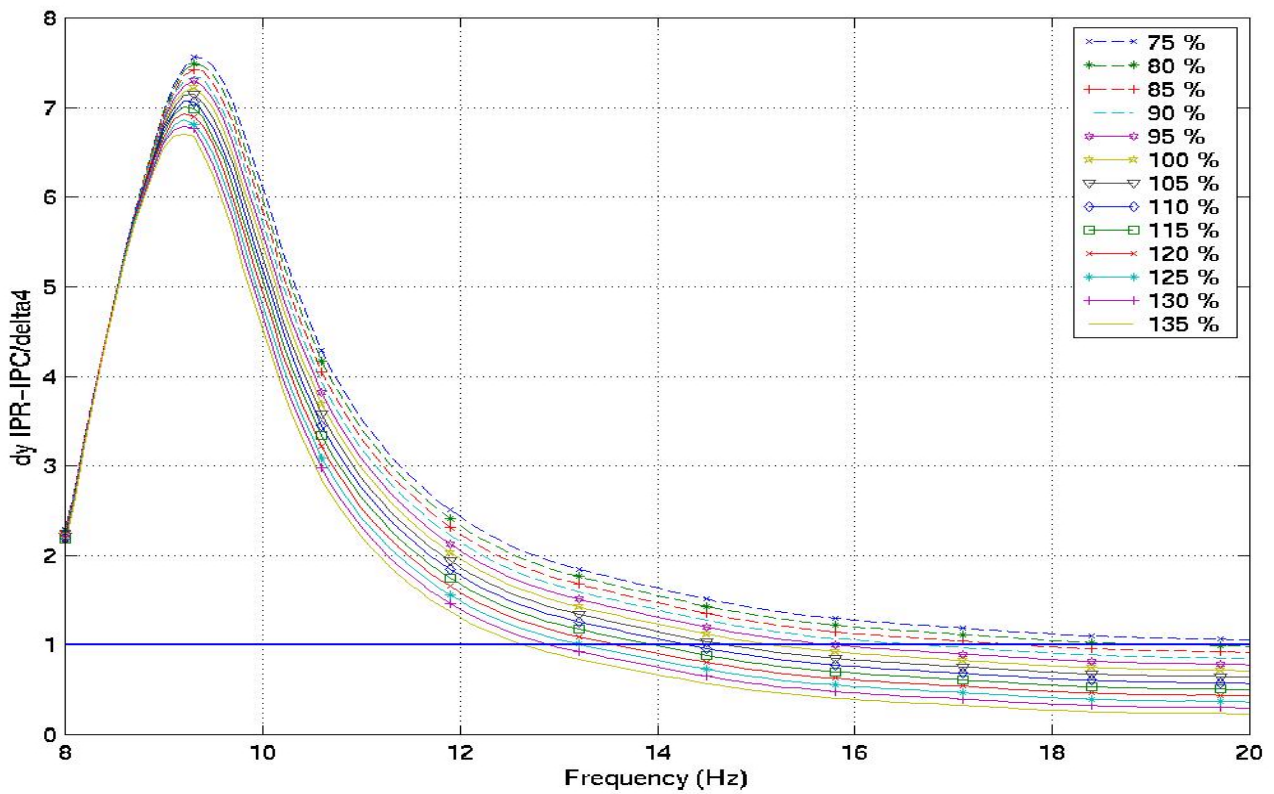

Fig 5 : Transverse relative IPR-IPC displacement when the LP-IP clearance varies from 75 % to 135 %, and the IPR-IPC clearance.
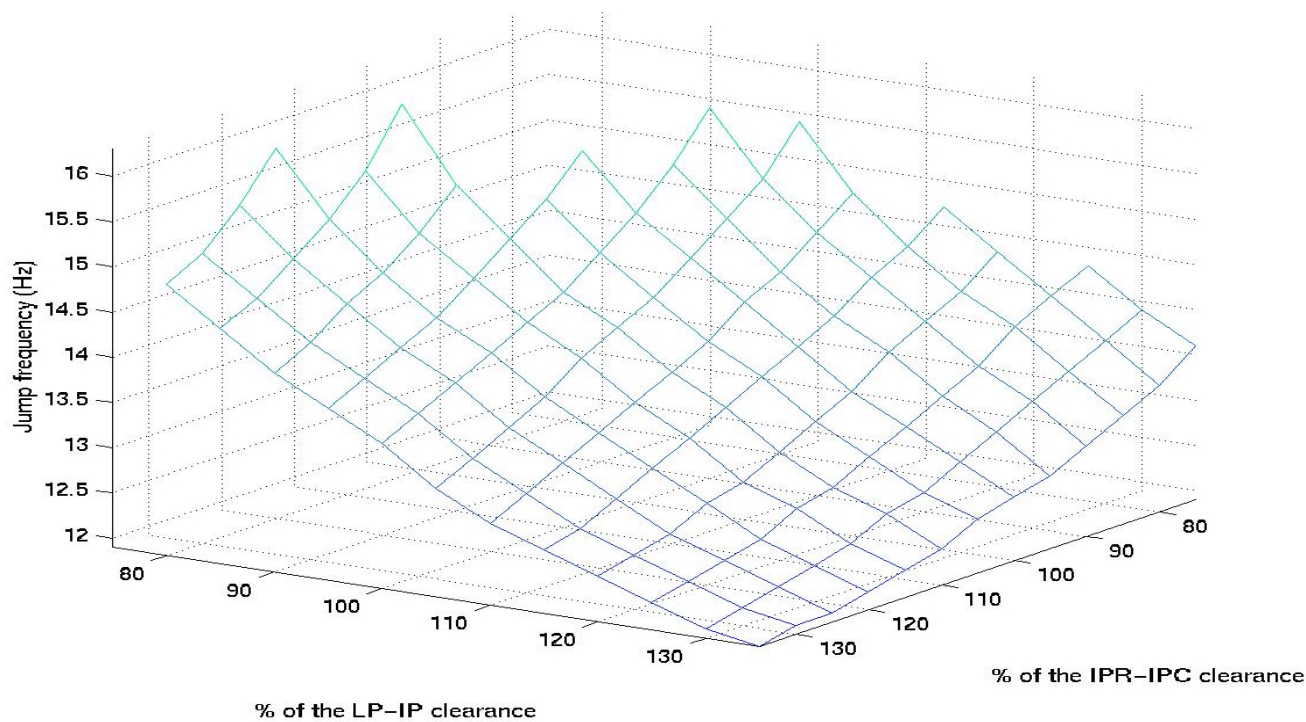
Fig 6 : Sensitivity analysis of LP-IP and IPR-IPC clearances on the jump frequency